POLITECNICO DI TORINO
Repository ISTITUZIONALE

Compliant assembly tolerance analysis: guidelines to formalize the resistance spot welding plasticity effects

Terms of use:

Publisher copyright

(Article begins on next page)

06 May 2024

Compliant assemblies tolerance analysis: guidelines to formalize the resistance spot welding plasticity effects

Moos Sandro · Vezzetti Enrico

Abstract In the automotive field, the tolerance analysis is an important engineering design function aimed at improving the product quality and its assemblablity, reducing the overall costs and time to market.

Many studies concern with compliant assembly tolerance analysis, with the assumption of linear behavior (small deformations in the elastic range, isotropic material, constant stiffness matrix . . .) that is also applied when parts are joined with the widespread resistance spot welding processes. Conversely, technological studies of this joining process show that the parts are plastically deformed near the welding nugget.

Through the study and development of a FEM model that involves the plastic effects of the complete spot welding process, with parts subjected to dimensional and geometrical tolerances, this paper aims to analyse the peculiar effects of the joining method on the dimensional quality of a compliant assembly and defines guidelines to integrate them into a model for tolerance analysis.

A butt joint and a slip joint case studies are analyzed, applying tolerances that cause to two parts mismatching worst conditionss: gap and loading interference and measuring the residual spring-back of the parts according to a given Datum Reference Frame.

The analysis results show that the material plasticity induced by resistance spot welding and the Body-in-White process affect the assembly dimensional quality.

Keywords Compliant assembly · FEM · Tolerance analysis · Quality · Resistance spot welding

Moos Sandro · Vezzetti Enrico
Politecnico di Torino – Dipartimento Sistemi di Produzione ed Economia dell'Azienda (DISPEA).
Tel.: +39-11-5647294
Fax: +39-11-5647299
E-mail: sandro.moos@polito.it

1 Introduction

In the automotive field, the tolerance stack-up analysis is an important task [1], which is focused to improve assemblability and product quality, already from the first engineering stages of new projects, with the intent of highlighting and take methodological action towards the resolution of potential dimensional and geometrical problems, so to reduce quality related problems during prototyping, fixturing and production ramp-up.

The analyses are useful to support the definition of welding and assembly methods, production fixtures and control tools, to verify the reachability of the final results for the whole body of each sub-process and then set the tolerance limits for controlling the production lines, during production.

With a correct variational management it is possible to obtain a more robust design, to increase product quality, to reduce tool modification costs in pre-series and production validation phases and to reduce the adjusting costs of defective products.

Currently, many studies deal with compliant assembly tolerance analysis, with common assumptions of linear behavior (small deformations in the elastic range, isotropic material, constant stiffness matrix ...) also when parts are joined with the widespread resistance spot welding process (RSW).

However, other studies with a prevalent technological focus, shows clearly that plastic deformations are indeed present near the welding nugget. Though those papers does not analyze the full welding process with fixture and tolerance effects, they raise a doubt regarding the validity of linear behavior assumption in tolerance stack-up analysis.

To evaluate the role of plasticity in variational analysis for compliant assemblies, welded with RSW, this paper develops a set of guidelines to define a plastic analysis model,

which consider the principal Body-in-White (B.i.W.) process steps with the aim of providing a more accurate calculation of the tolerance stack-up.

To integrate both the dimensional quality problem and the technological parameters, for better evaluating the actual part springback when released from the welding fixtures, a FEM model has been developed to simulates a complete welding operation cycle (loading, clamps closure, heating, cooling, clamps release, fixture release and key points measurement according to a specific DRF - Datum Reference Frame).

In sections 1.1 the works concerning tolerance analysis on compliant assemblies are recalled to outline the aspects of the common formulation of linear behavior. In section 1.2, the papers concerning the welding of compliant parts are discussed to point out the plastic deformations caused by RSW process and to summarize the recent models, which do not consider parts tolerance.

In section 2 it will be proposed a model set-up to describe the whole B.i.W. process as an improvement of those recalled in section 1.1 and 1.2. The model will be applied to a case study regarding a butt joint in 3 and its result will be compared to some existing works in section 3.1, to provide validation. The extended results of the B.i.W. process will be discussed in section 3.2 and the results for a slip joint case study will be shown in section 4. The butt joint and slip joint have been selected for their wide use in the automotive field. The conclusion regarding plasticity effects will be drawn in section 5.

1.1 Variational analysis with compliant parts

In 1997, Hu and Liu had already outlined in [2] a mechanicistic FEM modeling of compliant parts to predict assembly variation, using the influence coefficients method to evaluate the parts' and whole assembly's sensitivity matrix. Then, in [3], Hu outlined a methodology aimed to the prediction of dimensional variation considering complex hierarchical assembly trees. The results highlighted that the propagation of variation during assembling is driven by the stiffness of the parts and sub-assemblies being assembled.

Other technical papers addressing the problem of defining a methodology for tolerance stack-up analysis of compliant assembly were developed: Liu et al. ([4]) proposed an offset beam element able to consider the shear stress provided by spot welding and also suitable for 1D assembly variation prediction.

In [5,6], Hu et al. combined engineering structure analysis with statistic methods to consider the effects of parts and tools variations, clamping deformations, joining and springback.

Chang et al. ([7]) grouped parts and tooling as features from which variations and displacements were represented by contact chains and were propagated by vector equations considering geometric compatibility, force continuity and constitutive relations at nodes.

Hu et al., in [8], proposed a FE method based to calculate spring back effects in a butt joint considering the complete B.i.W. process and with the assumptions of friction free and linear behavior. The real springback of the parts, once released from the fixture, is sketched in figure [8, fig. 4d]: the part returns to an undeformed shape with u_x equal to the initial gap δ_u and a vertical displacement u_y which is mainly determined by the boundary condition sketched in [8, fig. 4b], namely one electrode is still and the other deforms the left part only. u_y is evaluated in that deformed condition [8, fig. 4e]. This approach will be recalled in section 3.2 for a more detailed comparison to the result of the present study.

Chen et al. considered in [9] a geometrical model with parts deformations and tools variations, which highlighted the different sensitivity of an assembly to slip joints or butt joints and so the importance of a properly designed product structure and process fixtures.

Byungwoo et al. presented in [10] an approach to integrate the Datum Flow Chain analysis ([11, 12]), with a commercial 3D variation analysis software (3DVA) and FEA. The first step of the proposed method is to define the compliance and sensitivity matrix of each parts by means of influence coefficients ([2]). The sensitivity matrix is computed once for all by FEM, with the parts located on a set of isostatic locator and then applying an unit displacement to the overconstrained joint at each part. The forces and deformations are stored. The compliance matrix of the whole assembly is computed similarly applying a unit force on each joint. The displacement resulting on the control points can be defined as a linear combination of the effects computed on parts and assembly. The approach is well suited for Monte Carlo simulation, to calculate the probability function of variations and their contributors.

Fan et al., in [13] "superimposed" the local spot welding plastic distortions to a nominal FE assembly mesh, with welding flanges in matching condition. The simulation predicted the same mode of deformation experimentally measured on real parts: a distortion of the assembly with a twist induced around a diagonal axis, but underestimated the magnitude. The deformations measured on the assembly were also compared with the variational simulation made with TAA software, which considers the parts deviation from their nominal dimension with an elastic model and the results show a different deformation profiles. The suggested approach for obtaining more accurate simulation, is to combine local joint distortion with the elastic global deformation of components. The paper does not considers the parts deformation necessary to couple the welding flanges which are subjected to tolerances.

In the aircraft field, Saadat et al. ([14]) set up an experimental rig for large deformable aluminum components, in which simulated the load the external wing panel apply to any of the internal reinforcement rib and measured its deformations.

These loads come from the parts' mismatch due to manufacturing tolerances and cause a lateral deformations of the ribs which make difficult fastening and other final assembly operations. A rib FE model was set up with constraint and loads similar to the ones of the experimental rig and the calculated displacement of control points resulted similar to the measured value.

Other papers studied the definition of the contact properties between parts: Liao et al. applied in [15] a fractal geometry approach to model the variation of surface micro-geometry of parts being assembled, that is used in FEM to evaluate the final assembly variation. It is shown that different tool-releasing schemes produce different assembly variation distributions which can also be asymmetrical and that micro-geometry of assembly components should not be neglected for high precision assemblies.

The results were further expanded in [16] were a wavelet methodology was employed to identify different scale components of part variation in the tolerance zone. And in [17] it has been set-up a method to simulate correctly the contact problem with contact FEM, also considering the friction forces between assembly surfaces. The study showed a weak dependence of the assembly dimensional variations on friction coefficient parameter.

Other authors dealt with a proper fixture design: in [18] Camelio et al. developed a designated component analysis to extract from production data the significant variations patterns and correlated them to the fixture faults while in [19] focused on an optimization algorithm which combines FEA, to consider the effect of part variation, tooling variation and assembly springback. Nonlinear programming methods were used to determine the optimal fixture position to minimize assembly variations.

The problem of tolerance synthesis has been considered by Manarvi et al. in [20], where they presented a framework to gather available information to develop an integrated tolerance synthesis model, based on assembly architecture and manufacturing process, with FEA to predict the influence of geometric tolerances on part and assembly distortions.

In [21], Li et al. applied the analytical target cascading process to the tolerance allocation problem, translating the nal product variation targets to tolerance specifications for subassemblies and single parts. The part deformability effect on assembly variations has been considered by FEA.

Other aspects were considered by Camelio et al. ([22]), which used the principal component analysis to extract from production measure the part covariance, the deformation patterns and their contributors. FEA has been used to determine

the effect of each deformation pattern on the global assembly variation.

Wang et al. proposed in [23] a method to define the optimal assembly sequence so to optimize a multivariate process capability index, considering the variation propagation with compliant parts.

Maropolous et al. ([24]) highlighted the importance of assessing the dimensional variation of compliant assemblies, which should be considered as one of the many design activities to be carried out and maintained in the perspective of Product Lifecycle Management.

In [25] Sodeberg et al. emphasized the importance of Visual Quality appearance and presented tools for non-rigid variation simulation and photo-realistic presentation capabilities, to guide the Virtual concept verification.

To summarize, the above mentioned methodologies [4–10, 14] assumed the sheet metal deformation being in the elastic range, with isotropic material, neglected thermal deformations and considered the stiffness matrix as constant and linear, for small part deformations.

An approach to reduce the computation time, proposed by [10], is to firstly perform a FEA to calculate the stiffness matrix with influence coefficients that is later used for variation calculation with Monte Carlo simulation, instead of running a FEA for many simulations.

[13] is the only work which starts to consider some welding plastic distortions effects on the parts geometry.

Moreover, [15–17] showed the importance of parts contact to obtain a better modeling of the compliant behavior; [18, 19] outlined the effects of the fixtures on assembly quality, [22, 23] pointed out the importance of the loading sequence and [24, 25] discussed the positive effects of a correct tolerance management and representation in the product life cycle.

By contrast, after recalling the papers that analyze variational problems with elastic models, in the following section are reviewed those papers modelling the welding process with particular attention to the plastic deformation present near the welding nugget.

1.2 Spot welding modelization

Spot welding has been deeply analyzed for many purposes: in the mechanical field to define and model the mechanical strength or the fatigue behavior, while in the technological field to define the optimal process parameters.

Huh et al. in [26] modeled the welding process considering the specific heat variation during melting, the heat generated by Joule effect, the electric current density governed by Quasi-Laplace equation, for electric potential, expressed in the parts' volume and on the contact surface and the heat transfer inside parts by conduction.

The section and thickness of the welding nugget have been calculated with 3D FEA for elliptical and cylindrical electrodes geometry, concluding that the cylindrical electrode produces the largest nugget under the same welding conditions, while strongly elliptical electrodes degrade the nugget dimensions.

Feng et al., in [27], considered the electric contact conductivity dependent from the electrode-to-sheet and sheet-to-sheet contact pressure. The results show that after few welding cycle, the electrode tip is flattened, then the nugget formation is greatly delayed because the heating moves toward the periphery of the contact region and the effect is stronger for thicker sheets.

The pressure graph of the contact pressure versus radial distance also shows that the heating of the first few welding cycles cause a thermal deformation which reduces the contact area, when temperature further rise. The material softening induced by the temperature raising provide a leveling of contact pressure.

In [28], Zhang et al. considered the welding of sheet parts with an initial gap through a thermal-elastic-plastic sequentially coupled FEA. The conclusions show an initial mismatch between electrode and sheet, caused by the part deformation, that will start a delayed nugget formation, with a ring shape, so negatively influencing weldability.

Eisazadeh et al. simulated in [29] the nugget formation and the effects of the process parameters on it (welding current, welding time, sheet thickness and material, electrodes geometry and closing force, current shunting).

It quantified and concluded that electric flow should not exceed an optimal flow limit for nugget growth, otherwise the nugget size raises until melt spattering occurs. To reduce the current shunting effects the spot weld locations should be spaced above a minimum distance.

Increasing welding times brings to a bigger contact surface and a bigger nugget, while increasing the closing force of electrodes decreases the nugget size because it raises the contact surface area. Increasing the plate thickness also require a bigger current flow, needed for an appropriate weld nugget formation. Decreasing the plate thickness lowers the electrode diameter.

In [30], Hou et al. with a 2D axisymmetric model of coupled thermo-elastic-plastic FE model investigated the mechanical behavior of spot welding process considering temperature dependent properties and plastic behavior of materials.

The calculated history of the contact pressures showed high pressure values around the border of the faying surface and at the border of the electrode-workpiece contact. During the welding cycles, the stress component along welding axis was of high compression in the contact area of faying surface.

The deformation of the weld near the electrode border, the detachment of welded sheets and the electrode displacement due to the thermal expansion and contraction were also described.

Ranjbar et al. ([31]) with a 2D electro-thermo-mechanical model predicted temperature and residual stress distributions during different stages of resistance spot welding.

The model results, when compared to measured residual stresses, showed good agreement: the circumferential residual stresses are tensile in the weld center and change to compressive state towards the edge of the sheet.

The radial residual stresses are tensile in the weld center and compressive at the border of the nugget. Higher welding times lead to reduced tensile residual stresses, while increasing the welding voltage, brings to enhancing the tensile residual stresses.

Kong et al., in [32], defined a detailed FE model in which the spot weld was divided into sub-zones with different material properties (particularly yield and strain hardening) due to the thermal, metallurgical and mechanical deformation process.

The 3D FE model coupled with a fracture model predicted the deformation of spot-welded slip joints well beyond initial yield under tensile-shear loading. The computed deformation mode and force-displacement data were in good agreement with experimental results.

Rahman et al. defined in [33] a sample spot weld element with shell/plate, beam and rigid elements, able to transfer from one mesh to another the membrane and bending stresses. The application of the spot weld element on a slip joint and butt joint, with a load time history, allowed the analysis of the fatigue behavior of RSW sheets under variable amplitude loading and highlighted how the spot diameter and thickness greatly influence the fatigue life of spot welded structures.

Other authors dealt with the problem of parts and electrodes contacts: Feulvarch et al. ([34]) defined a electro-thermal contact model suited to improve the calculation of the heat flux due to dissipation effects when the meshed electrode-to-sheet nodes are not linked face to face, so allowing independent mesh dimensions on parts and large displacement between contact surfaces.

In [35], Song et al. experimentally measured the electrical contact resistance of mild steel, stainless steel and aluminum, considering different contact pressures and temperatures. It is clearly shown that contact resistance decreases with pressure, while the temperature role is complex.

Other informations regarding the modeling of spot welding process were provided by Yeung et al. in [36], where performed a thermal analysis of welding caps cooling and also evaluated that convective and radiant heat losses outside the electrode are negligible.

The above papers mainly considered geometrical matching between sheets and focused only on technological properties of RSW and mechanical properties of welding nugget. The initial part mismatch problem has been dealt with by [28] but only for the consequences on welding nugget dimensions.

These detailed and complete analysis are a starting point to integrate the plasticity effects of RSW into assembly variation evaluation.

2 Resistance spot welding modelling including parts subjected to variations

Considering the effects hinted by the results of [13] for the effects of the welding distortion on the assembly and those of [27, 29, 30, 34], where a local detachment of the welded parts was clearly shown, this paper will evaluate the importance of the effects of thermal deformations and plasticity in the welding area.

To accomplish this aim, it has been developed a FEM model able to investigate the whole B.i.W. process with a variational point of view, considering parts deformations and spring-back resulting after a RSW with a plastic material model. This has to consider parts with geometrical and dimensional tolerances on their welding flanges, defined according to a specified Datum Reference Frame.

Of all the tolerance combination of the flanges being welded have been considered the conditions that present the maximum allowable gap and the maximum loading interference, being those the opposite worst cases.

The phases of fixture clamping, weldgun closure, heating, cooling, weldgun opening and fixture release are simulated and the measurements of the deformed assembly are made accordingly to a prescribed DRF.

The approach is described in figure 1: the analysis has been computed in three stages using different models with a set-up suitable for common FEM software without requiring the implementation of dedicated co-simulation solutions.

A first general static analysis computes the deformed configuration of the sheets caused by weldgun closure, stopping just before welding. The second FEM model performes the calculation of the temperature field during RSW on the deformed shape previously calculated. The third model imports the temperature distribution from the second model and continue the simulation past the end of the first model.

In the first model, the DRF prescribed on drawing and implemented as a set of locators on the fixture is translated into equivalent boundary conditions applied to the parts.

A schematic example of a fixture is shown in figure 2, where on the fixture base are positioned the locator supports for the sheet parts in the Y (vertical) direction, two pins will fit in the hole/slot couple of each part to prevent rotation around Y axis and translations along X, Z axes. When
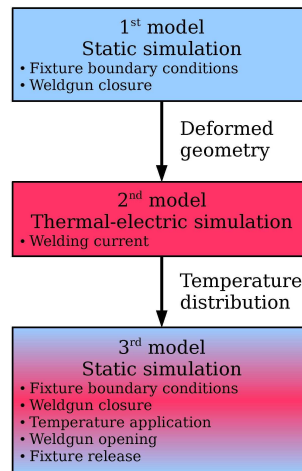

Fig. 1 Analysis set-up.

closed, the movable clamps will lock the sheet against the locator supports preventing any other movement.

On parts are defined the mesh partitions with the shape, size and orientation of the corresponding clamps. The play between the fixture's pins and the part's holes and slots has not yet been considered because its contribution mainly change the initial gap/interference dimension, so it's not fundamental for the description of the process at this stage.

Figure 2b shows the worst case condition with both parts at minimum dimension, within the tolerance range: between the two flanges is present a gap that will be closed by welding guns during the squeezing phase. For this gap condition, on the locators are applied encastre boundary conditions, considering that the clamping force and the friction are enough to prevent any further motion of the parts.

Figure 2c shows what would be if the two parts were in the opposite worst case condition, when both were at the maximum dimension within the tolerance range. The compenetration is physically impossible, so the last loaded part will assume a position like the one sketched in figure 2d: the back side rest on the fixture locator and the bending radius of the flange lean on the vertical flange of the other part.

For the interference condition, the parts are manually positioned considering the loading sequence: the first part is completely laid down on the fixture, then the following part is placed partially on the first one and partially on the fixture, by mean of adequate rotations and translations. The mesh partition on the second parts which will not be in contact with the fixed locator of the fixture will be moved by mean of prescribed boundary condition to their nominal position to simulate the clamping and there locked. The deformation work will store some elastic energy into the parts and a plastic deformation where the stress reach the yield limit. This elastic energy will be released on clamp opening and cause springback effect, while the plastic deformations alter permanently the geometry.
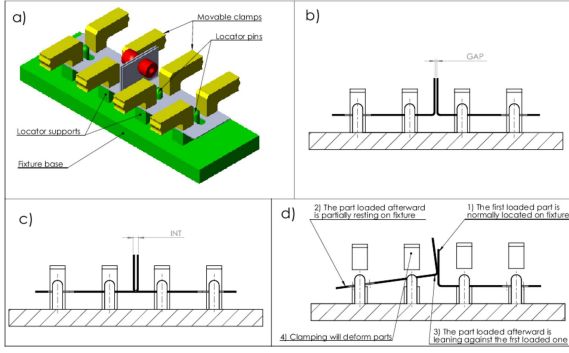
Fig. 2 Parts positioning on fixtures.)

Parts are modeled with the dimensional and geometrical defect and are meshed with solid elements. It is not possible to adopt a shell representation under axial-symmetry conditions because it is invalidated by the weldgun deformation. The mesh dimension has been chosen as a compromise between simulation time and results precision.

The contact property defined for sheet-to-sheet and electrode-to-sheet interface considers an "hard contact" for the normal behavior and friction for the tangential one.

Weldgun closure is performed by mean of an initial displacement that brings the nodes of the electrodes in contact with the sheet, than the closing force is applied.

The simulation of the slip joint has been set-up similarly to the butt joint model: figure 3 shows the parts loaded on fixtures, subjected to the opposite tolerance situations: fig. 3a is the case with a mismatching gap, while fig. 3b is the case with the parts in a loading interference condition.
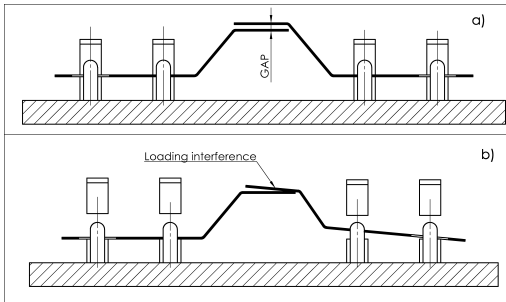

Fig. 3 Parts positioning on fixtures for sliding joint.

For the general static analyses, the materials properties of elastic modulus, expansion coefficient, plastic strain and plastic yield are temperature dependent, accordingly to the data previously employed in literature. The chosen plasticity model is isotropic with Mises yield surface formulation.

The first model only computes the parts' deformed shape at the end of the squeezing step, considering the plastic deformations, that will be exported as "orphan mesh" to the second model in which is performed a coupled thermal-elec-

tric simulation to calculate the temperature distribution during the welding and cooling phases.

The electric field in the conducting material is described by Maxwell's equation of charge conservation for steady-state current (combined the Ohm's law $\mathbf{J} = -\sigma^E \cdot \frac{\partial \phi}{\partial \mathbf{x}}$) and it is coupled with the energy balance equation that describes the heat conduction:

$$-\int_V \frac{\partial \delta \phi}{\partial \mathbf{x}} \cdot \sigma^E \cdot \frac{\partial \phi}{\partial \mathbf{x}} dV = \int_S \delta \phi J dS + \int_V \delta \phi r_c dV, \quad (1)$$

$$\int_V \rho \dot{U} \delta \theta dV + \int_V \frac{\partial \delta \theta}{\partial \mathbf{x}} \cdot \mathbf{k} \cdot \frac{\partial \theta}{\partial \mathbf{x}} dV =$$

$$= \int_V \delta \theta r dV + \int_S \delta \theta q dS. \quad (2)$$

where V is a volume of surface S of normal $\mathbf{n}$ positive outward, ϕ is the electrical potential field, $\mathbf{J}$ the electrical current density, $J = -\mathbf{J} \cdot \mathbf{n}$ the current entering S surface, r_c the internal volumetric current source per unit volume, $\sigma^E(\theta)$ the electrical conductivity matrix, θ the temperature, $E = -\frac{\partial \phi}{\partial \mathbf{x}}$ the electrical field intensity, ρ the material's density, U the internal energy, $\mathbf{k}$ the thermal conductivity matrix, q the heat flux per unit area flowing into the body and r is the heat generated inside the body.

The electrical and thermal problems described by equations 1 and 2 are coupled by the temperature dependence of the conductivity in the electrical problem and by the electrical current dependence of the internal heat generation in the thermal problem. In fact, the Joule effects is the heat source inside the material volume: $r = \eta P_{cc}$ with $P_{cc} = \mathbf{E} \cdot \mathbf{J} = \mathbf{E} \cdot \sigma^E(\theta) \cdot \mathbf{E}$ and η an energy conversion factor.

The external surface S of the body can be divided into patches for which boundary conditions can be prescribed and patches that interact with surfaces of other bodies. The boundary conditions regarding the electrical potential $\phi = \phi(\mathbf{x},t)$, temperature $\theta = \theta(\mathbf{x},t)$, electrical current density $J = J(\mathbf{x},t)$, heat flux $q = q(\mathbf{x},t)$ can be directly specified.

The heat conduction across the surface interfaces of different parts is modeled considering a gap thermal conduction coefficient k_g: $q_c = k_g(\overline{\theta})(\theta_B - \theta)$ and similarly the electrical current flow $J = \sigma_g(\theta)(\phi_B - \phi)$, can be modeled with a gap electrical conduction coefficient σ_g. θ_B is the temperature of adjacent body's surface, ϕ_B its electric potential, $\overline{\theta} = \frac{1}{2}(\theta + \theta_B)$ is the average temperature at surfaces of the two bodies.

In the welding step, an alternating current is imposed on the rear surface of an electrode for the duration of the welding time and a zero potential is applied on the opposite electrode. Passed that time and stopped the current, the cooling step only considers heat conduction inside parts' material. Thermal convection and radiant heat losses were neglected accordingly to [36]. All the physical parameters involved are temperature dependent.

The third model is a general static analysis that executes all the B.i.W. process, importing the temperature distribution from the second analysis as a predefined field, for the heating and cooling phases.

The portions of the parts meshes that passed the melting temperature at the end of heating step are manually identified in a set and during the cooling phase they are locked together changing the contact properties, to simulate the joining effect. The weldgun is opened firstly removing the squeezing force, then applying a displacement.

The fixture release phase is implemented by removing the constraint on sheet parts according to the DRF for the assembly measurement.

The model set-up here outlined, will be applied and discussed in detail in the following case study.

3 Butt joint case study

The FE models of the butt joint will deal with the geometrical condition described in figures 2b and 2d with the aim of measuring the deformation induced by clamping and welding, after fixture release.

A common datum scheme has been used through the complete assembly process: part tolerance specification, welding and assembly tolerance measurement, to achieve a better understanding of the measure results.

Figure 4a shows the datums used to clamp two sheet metal parts shaped for realizing a butt joint; here, the locator scheme for the assembly consists in four local datum to define the parts position in the Y direction (A1-A4); one hole (B) coupled with one slot (C) define the Z position and the hole (B) also define the part position in the X direction. The same DRF has been repeated for the other part (D1-D4, E, F). The parts are not in the nominal conditions being each joint flange subjected to the form tolerance shown in figure 4b, defined using a DRF similar to the assembly's of figure 4b. Finally, the assembled parts are measured using the DRF shown in figure 4c.

For the static analysis, the datum references of figure 4a and the fixture shown in figure 2a have been further simplified into the FE model. Considering figure 5, the boundary condition enforced by Y locator have been realized locking the Y displacement of a transversal band at the end of each sheet, the effects of the pin/hole and pin/slot locators have been modeled locking the XZ displacement of the sheets rear section. The weldguns have been constrained so that only X motion is available and on their rear side has been applied a pressure equivalent to a welding force of 2500 N.

The sheet geometry has been defined considering the dimensions shown in [28]. Sheets and weldgun have been meshed using 3D stress C3D8 elements from Abaqus/Standard library.
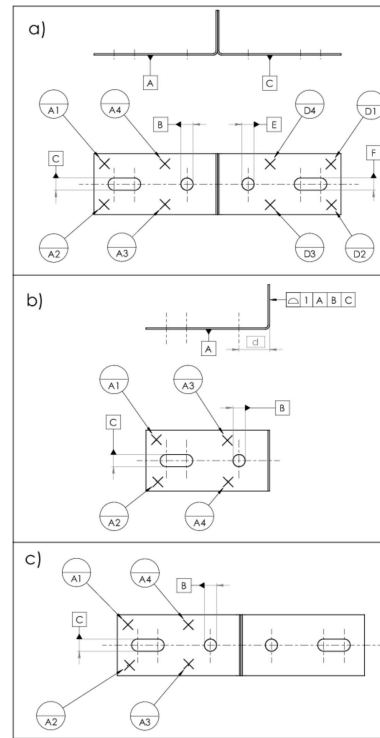

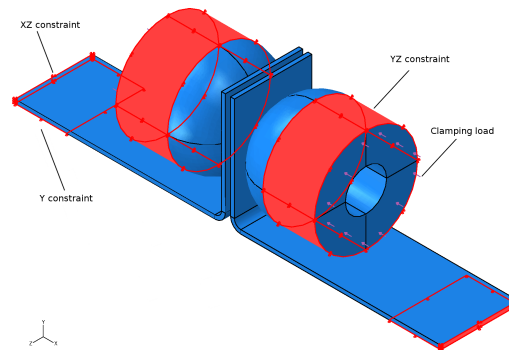**Fig. 4** Datums reference frames for parts, assembly and measurement.

Fig. 5 FEM model with boundary conditions.

As sheet thickness, it has been chosen 0.75 mm, which is often used for body-side parts, frames, rear light housings, some parts of upper rails in under-body. The sheet-to-sheet and electrode-to-sheet contact pairs were defined using surface to surface enforcement. Friction was considered between contact pairs: $f_{Fe/Fe} = 0.11$, $f_{Fe/Cu} = 0.53$ and the other material properties were retrieved from [30].

The specifications for thermal and electrical bulk conductivity, specific heat $c(\theta) = \frac{dU}{d\theta}$, latent heat, gap thermal and electrical conductance at surface interfaces, where took from the same source [30]. On a rear side of an electrode has been defined an alternating surface current equivalent to 7900 A, with 50 Hz frequency and on the opposite electrode a potential of 0 V has been set. The heating phase duration has been considered 0.15 s and it is followed by a cooling phase of 0.6 s.

The fixture release phase has been implemented by progressively removing the constraint only on a sheet part: the XZ constraint are released first so to evaluate the springback in the X direction only, then the Y constraint is also removed to evaluate the overall springback. The other part has been held on the constraint to simulate the measurement phase, in which a reference system for measure is fit on the part considering the datums shown in figure 4c.

3.1 Comparison of butt joint results with other studies

The the butt joint with gap is the geometrical condition more similar to those analyzed in literature. Its results are here compared to those previously obtained, always considering an important difference of the model set-up: while the literature works solve the problem under an axial-symmetric condition given by parts matched together before the welding, the current model is not symmetrical around the welding axis because the contact surfaces are the result of the deformations imposed by the welding guns, on parts affected by tolerances. For this reason the results are always shown on two planes passing through the weldgun axis: the medial (vertical) plane Z and the Y (horizontal) plane.

The unsymmetric contact surface has a weak effect on the electrical current distribution shown on figures 6a and 6b. Because the sheets are matched above the electrodes they allow an higher electrical current flow than below. This will also cause an higher Joule heat generation above the electrode. The results are comparable with those of [29, fig. 13]. The electrical potential difference calculated at the end of the two clamps is 1.2 V.

The temperature distribution of figure 7b is comparable to those calculated by [29, fig. 8] and [31, fig. 4] for a sheet thickness of 1.52 mm and 1 mm respectively, though it is more flattened because of the smaller sheet thickness here considered.

This affects the temperature distribution in two ways: the cooling effects of the copper electrodes are more effective on the nugget given its narrow thickness and the heat production by joule effect is differently split between material resistance and contact resistance.

The equivalent circuit can be thought as a series of three resistors, the first and the last to consider the sheet resistance proportional to its thickness, the middle one to consider the contact resistance inversely proportional to the contact pressure [35, fig. 3,4,5].

Because the electrode force is adjusted on the base of the sheet thickness, it could results that the contact pressure does not vary much, in fact, the model results show a contact pressure of 80 MPa at the center of the faying surface and a maximum contact pressure of 91 MPa along a radial direction on Y plane, at the end of the clamping step, which are values corresponding to those determined by [30, fig. 5].
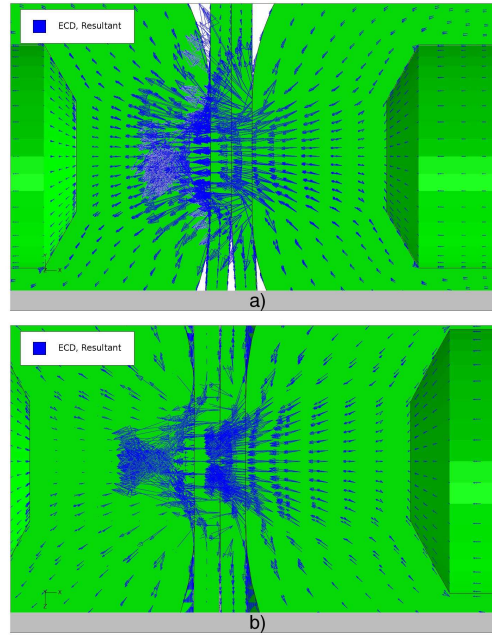
Fig. 6 Electrical Current Density distribution on a) Z plane and b) Y plane.

So, reducing the sheet thickness, the contact resistance plays about the same role for the joule heat production, while the bulk resistance decrease. The resulting temperature distribution is more similar to [30, fig. 3].

In the medial plane Z, the non symmetric contact condition plays an important role in the heat conduction, as can be seen in figure 7a. Above the electrodes axis the sheet are completely matched for all their length, while below the axis they are separated by a gap widening downward, so the first geometrical condition is more capable of heat conduction than the latter, thus leading to temperature distribution more extended above the electrode than below.

Figure 7a reports the temperature variation of the core node of the welding nugget during the welding time and the central node of the contact interface of sheet and electrode. Comparing this result to [30, fig. 4] and [29, fig. 9] are evident some differences.

The heating time is shorter than those calculated on other studies for the smaller thickness of the welding sheets. The temperature of the sheet/electrode node reach about 450-°C and the node at the center of the faying surface reach 2115 °C. In [30] the values are respectively about 775 °C and 2050 °C while in [29] the temperatures reach about 1000 °C and 2000 °C.

The Von Mises stress distribution of figure 8b is similar to the one obtained by [29, fig. 6] and it is confirmed that the maximum stress occurs at the border of the contact surface between the electrode and the sheet. Figure 8a show a clear disuniformity of the Mises stress: at the lower end of the sheets contact there is a bigger section of material sub-
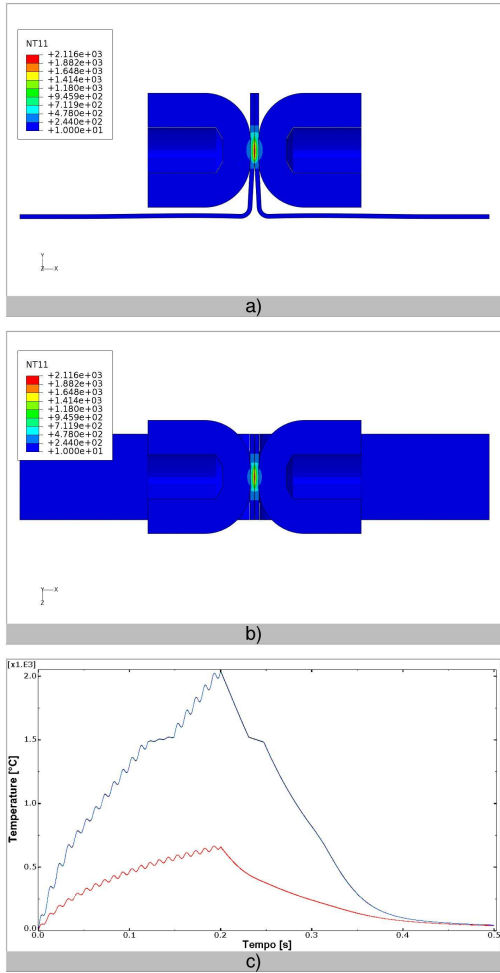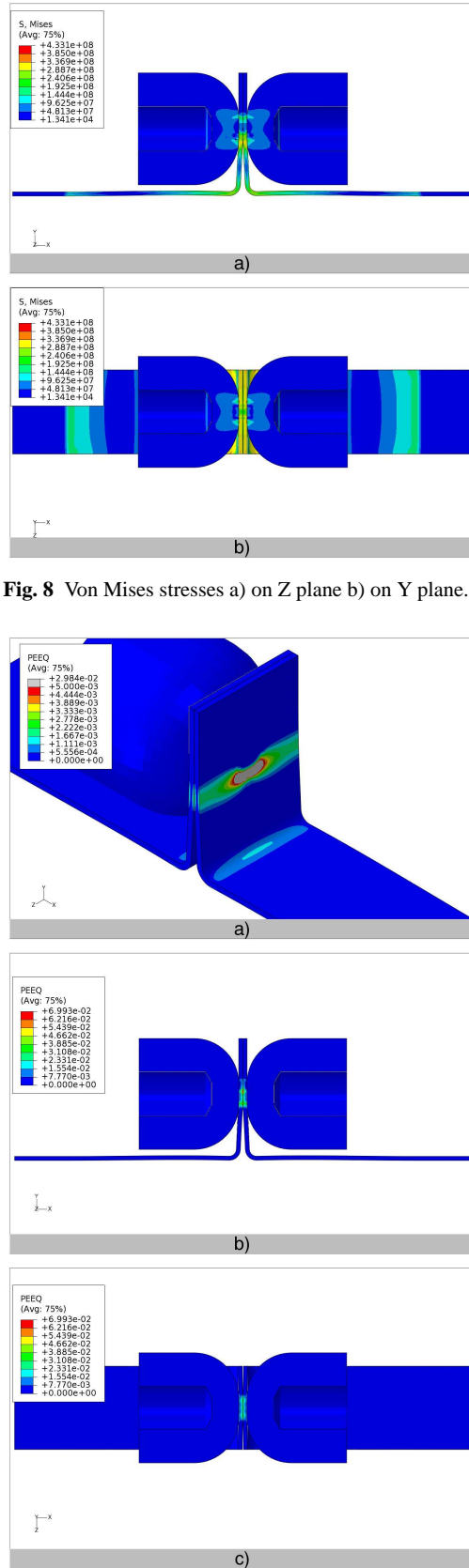
Fig. 7 Temperature distribution on a) Z plane and b) Y plane. c) Temperature variation at the core of the welding nugget and at sheet/electrode interfaced as function of welding time.

Fig. 8 Von Mises stresses a) on Z plane b) on Y plane.

Fig. 9 Equivalent plastic strain (PEEQ): a)distribution on the sheet surfaces, b) on Z plane, c) on Y plane

jected to high stress values, because those elements are the first to be deformed during the initial closure of the welding electrodes against the sheets. The figure also shows a stress distribution along the sheet thickness due to the bending deformation imposed by the electrodes.

Figure 9a presents the results of equivalent plastic strain distribution (PEEQ) which is defined as $\left.\overline{\varepsilon}^{pl}\right|_0 + \int_0^t \dot{\overline{\varepsilon}}^{pl} dt$. Each part shows large plastic zones: immediately below the electrode axis there is a large deformed area, which is laterally extended on both sides of the electrode and there is also a permanent deformation near the fillet between the vertical flange and the horizontal plane of the sheet.

Though the mesh resolution is small, in section 9c it is recognizable a plastic strain concentration near the border of sheet/electrode contact, like in [30, fig. 9], while section 9b shows again a larger deformation at the lower end of the sheets contact which is congruent to the results of Von Mises stress in figure 8.

Table 1 Comparison of the result with existing studies.

Case study results		Other study results	
Electrical potential difference	1.2 V	[0.88; 1.53]V	[31]
Sheet/electrode temperature	450 °C	775 °C	[30]
		1000 °C	[29]
Faying surface center temperature	2115 °C	2050 °C	[30]
		2000 °C	[29]
Contact pressure at the center of the faying surface	80 MPa	85 MPa	[30]
Maximum contact pressure around welding nugget	91 MPa	90 MPa	[30]

Table 2 Correspondence of the field variables with existing studies.

Case study results	Fig	Other study results	Comparison
Electrical current distribution	4a	[29, fig. 13]	Slight unsymmetry
	4b		Comparable
Temperature distribution	5b	[29, fig. 8]	Comparable
		[31, fig. 4]	Comparable
		[30, fig. 3]	More comparable
	5a	//	Unsymmetric
Temperature transient	5c	[29, fig. 9]	Comparable, lower electrode temperature
		[30, fig. 4]	
Von Mises stress	6a	[29, fig. 6]	Unsymmetric + bending
	6b		Comparable + bending
Plastic strain	7a		More plastic deformation below electrode contacts
	7b	[30, fig. 9]	Comparable
	7c		Sheet parts are deformed outside welding nugget area

Figure 9 shows analogies and evident differences to the other studies of welding simulation [29–31, 34], the latter to be attributed to the initial part mismatch that should be considered when dimensional and geometrical tolerances are present.

Considering also the condensed comparison of the results provided by tables 1 and 2 it is possible to conclude that the proposed model setup is able to consider the main aspect of the welding process.

3.2 Detailed analysis of butt joint results

Other important aspects of the welding process that influence the geometrical and dimensional quality of the joined parts are taken into account with the complete welding process simulation of both gap and interference condition. The plastic behavior is described in figures 10, 11 for each process phase.

Starting from the initial worst condition in which the parts present a gap for the dimensional and geometrical mismatch of figure 10a, the electrodes are closed against the vertical flanges and bend one toward the other. This produce a bending stress distribution which will be superimposed to the other stresses calculated in the other process phases (figure 8).

After the upper trim of the two flanges have made contact, the contact constraint makes the vertical flange to re-

verse bend under the electrode effect and shortly determines material plasticization, particularly concentrated at the lower border of the electrode/sheet contact area. The plastic area grows to the limits of figure 10b, where the weldgun is completely closed and applies the total welding force.

Then, the heating caused by the welding current makes the material near the electrodes to become plastic 10c.

After the parts cooled down and the welding gun is removed 10d, it is possible to identify a slight vertical springback of the welded flanges, directed along Z-, of 0.66 mm. This vertical displacement calculated considering the analytical solution of [8, eqn. 1] for elastic material, will lead to an overestimated result of 0.85 mm (with $a = 30$ mm, $b = 12$ mm, $\delta_u = 0.5$ mm for each part).

To simulate the CMM measurement, the constraints of one sheet have been removed in the FEM software accordingly to the datum system specified in figure 4c. The removal has been performed in two stages, the first to evaluate the X springback in the welding direction 10d, the second to completely free the sheet.

The X springback resulting from the plastic simulation, removing the corresponding constraint, is equal to -0.22-mm. When the sheet is completely freed it is evidenced in figure 10e a rotation around Z axis of an angle of about 2°. This behavior differs from the one predicted with an elastic model by [8, fig. 4, 5]. The substitution of an elastic formulation of the material properties in this simulation would result in a completely different behavior: 1 mm horizontal springback and no rotation. The result calculated with plastic model is 78% smaller than the elastic one.

The results of the case described in figures 2c, 2d, when parts are in a geometrical and dimensional situation which hinders the loading onto the fixture, are shown in figure 11. The parts would compenetrate of 1 mm, so after the first part is normally loaded onto fixture, the second part lays down against the first one and only partially rest on the fixture fixed locator (fig. 11a).

In the first step has been simulated the effect of the fixture clamps closing on the sheets and deforming them into the expected position (figure 11b). Here, it is evident a first plastic deformation of the left sheet, near the edges of the clamping fixture constraint, which has a negative effect on the part geometric quality.

The parts behavior during squeezing step has been detailed in figures 11c and 11d. The left vertical flange is deformed by the electrode that push it on the upper contact point above the welding axis, so the flange will bend outward. At the base of the flange, just above the fillet, the bending cause a pronounced plasticization of the material.

The right flange is also bended outward in the other direction, by the contact with the electrode below the welding axis. The material at the base of this flange also become plastic, though with a smaller extent.
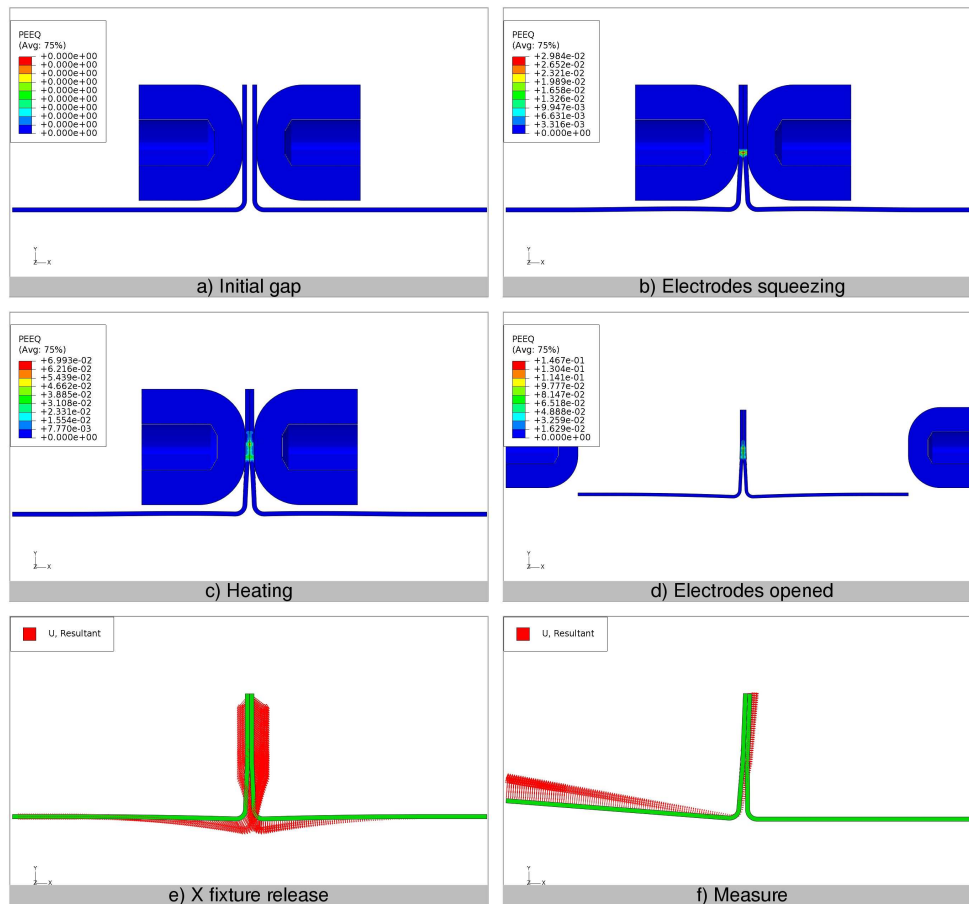
Fig. 10 Plastic deformation at the conclusion of welding steps. Gap condition.

The two flanges are bended and curved in opposite directions, so when the complete squeezing force is applied, they are counter-bended and another plasticization occurs in the right sheet near the lower contact border of the electrode.

The following thermal steps extends the material plasticization around the welding nugget (figures 11e, 11f).

When the left sheet is freed along X direction, as in figure 11g, the measured springback is +0.3 mm and at the upper edge of the vertical flanges occurs a displacement of 1.7-mm in X direction and -1.9 mm in Y direction.

After the complete release shown if figure 11h, the left sheet shows a considerable springback being -1.8 mm the Y displacement and $5°$ the rotation around Z axis. An elastic material model applied to this analysis would return an elastic springback of 1 mm and no rotation.

Both analysis of the butt joint found a notable plastic permanent deformation of the parts caused by electrodes squeezing (figures 10b, 11c–d) and in the case of loading interference also by fixture clamping (11b).

No approach found in technical literature has been explicitly set-up to consider the effects here described.

4 Slip joint case study

The results are summarized in figure 12 on pag. 13. The same material parameters, sheet thickness and DRF similar to those of fig. 4a-b-c were used.

For the slip joint, in a tolerance condition which provides a 1 mm gap between the two sheet parts (fig. 12a), it is evident that there is only a limited amount of plastic deformation, localized near the welding nugget (fig. 12b).

The figure 12c provides the measured displacements according to a DRF similar to fig. 4c: a vertical spring-back of 1.07 mm along Y- and a negligible X displacement are found. The deviation from an elastic prediction is about 7%. This confirms that the slip joint is less sensitive to variation propagation.

Due to the local plastic deformation caused by welding spot, the edges of the welded flanges are also distanced from the facing part of 0.13 mm at a distance of 10 mm from the welding axis, in the Y direction.

For the slip joint, with tolerances that provide a 1 mm loading interference (fig. 12d), it is evident the plastic deformation localized near the welding nugget (fig. 12e).
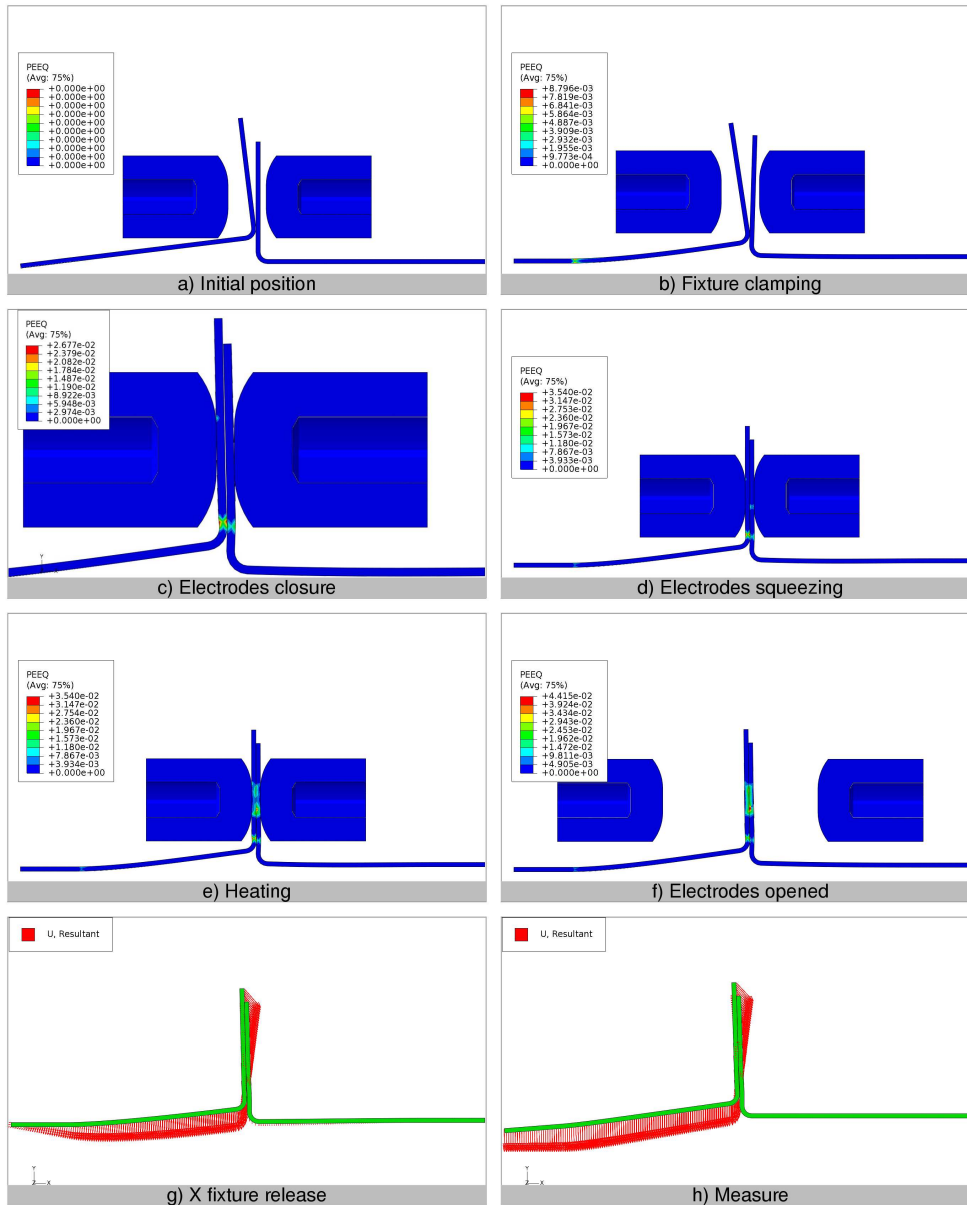
Fig. 11 Plastic deformation at the conclusion of welding steps. Loading with interference.

From the displacement represented in figure 12f, it is possible to determine a vertical spring-back of 1.29 mm on Y+, caused by the permanent deformation imposed by the electrode, which is 29% higher than the initial tolerance interference. In the same conditions, an elastic material model would foresee 1 mm of spring-back and no rotation.

Figure 13 provides evidence of a sliding phenomenon occurring along X direction, between the two sheet faces, during the electrode closure movement. The total slip measured once the weldgun are completely closed is quite significant, being about 0.67 mm.

This fact could be the source of more inaccuracy particularly for manual RSW processes, in which the welding gun is suspended on a winch and manually handled by the oper-

ator. If, for the force applied by the operator, the gun push in the vertical direction the two sheet it will cause an higher sliding between the two parts that will be made permanent by the welding spot. No previous literature work has been explicitly set-up to consider this effect.
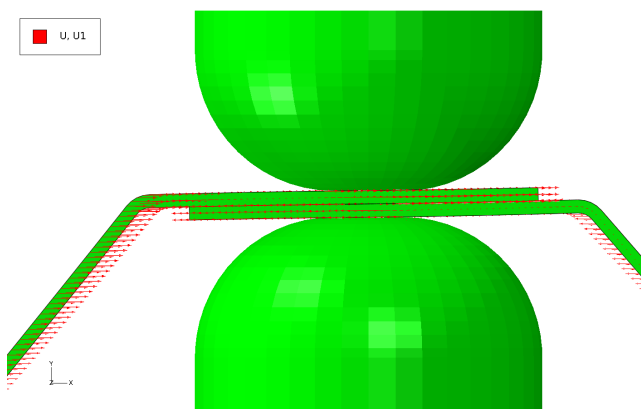
5 Conclusions

The results of the present model of RSW process show some peculiar behavior when parts are mismatching for tolerances reasons. The following phenomena occur when a butt joint presents a gap condition:
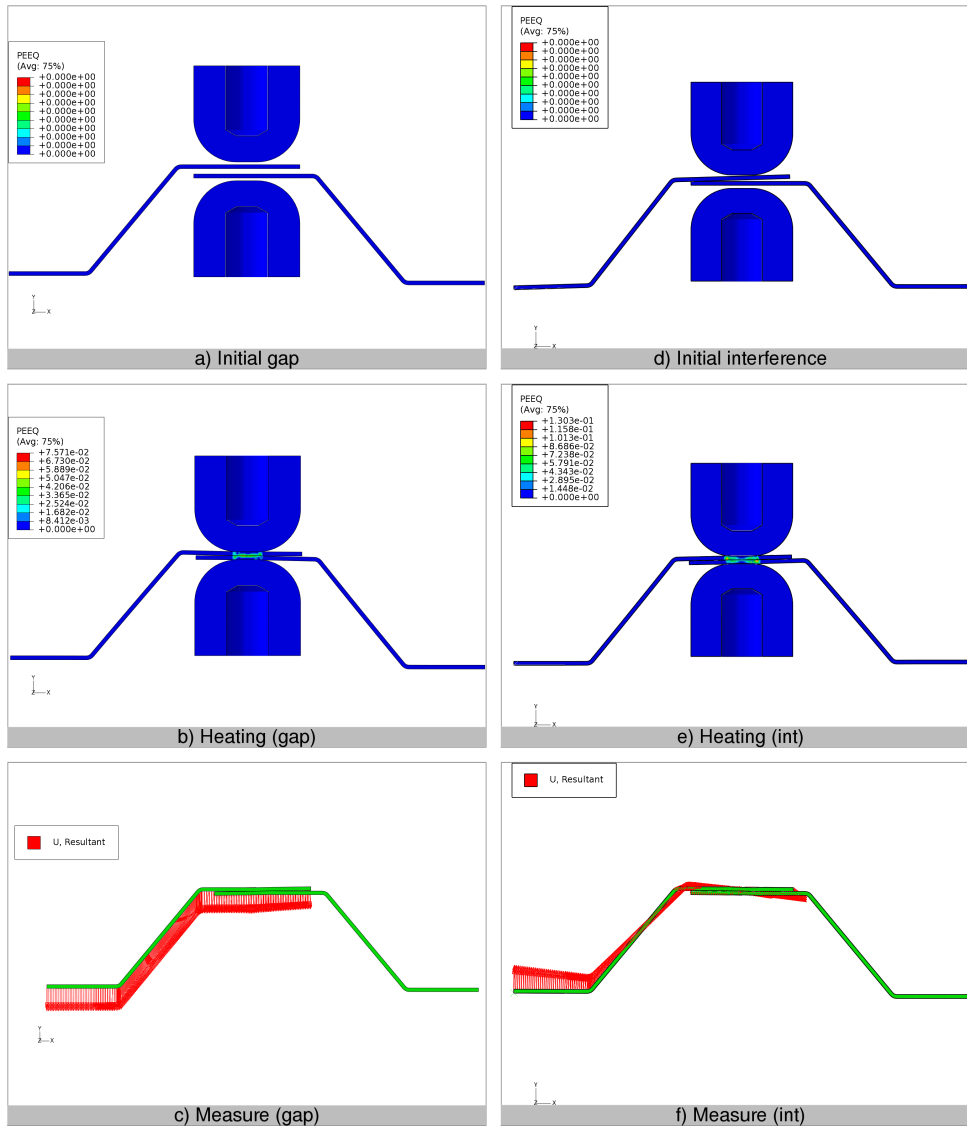
Fig. 12 Plastic deformation at the conclusion of welding steps. Gap and interference condition for slip joint.

Fig. 13 Sliding motion of the sheet parts along X direction during weldgun closure.

– plasticization near the fillet at the base of the welded flanges, caused by weldgun closure;
– the material plasticization significantly reduces the springback along the welding axis;
– it is present a bending moment near the welding nugget that causes a relative rotation of the parts when freed from the fixture.

In a butt joint which presents interference and cannot be correctly loaded on fixtures (fig. 11) occurs:

– plastic deformation caused by fixture clamping, with significant change to parts morphology;
– a more pronounced plastic deformation near the flanges' fillet;
– a reduced springback along the welding axis;
– a relative rotation of the parts.

The slip joint, characterized by a small stiffness in the welding direction, is far less sensitive to the phenomena described above. For the gap condition, the deviation of its behavior from the elastic model is almost negligible, provided a short tolerance stack-up, in fact:

- the plasticization is localized only near the welding spot,
- and there are no other plasticization hinges due to the small stiffness of the parts along the welding direction.
- It is evident a small distancing of the sheet edges due to the welding deformations.

The slip joint with interference condition presents:

- higher plastic deformations of the sheets being welded,
- increased spring-back after the fixture release, for the permanent deformation imposed be the electrode
- It also is evident a sliding motion of the parts during the weldgun closing, along tangential direction, that is made permanent by the spot weld.

With the results here described it is possible to define a ranking of the various joint based on their sensitivity to the plastic deformation: the butt joint with loading interferences could be subjected to the most extended plastic deformation imposed by fixture closing and welding, followed by the butt joint with gap condition, the slip joint with loading interference and the slip joint with gap condition. The more the parts are subjected to plastic deformation, the more unsuitable is an elastic tolerance stack-up model.

Comparing these results to the conclusion of [9] it is possible to derive other information:

1. the butt joint does not propagate the complete variation along the joint normal direction for the plasticity effect, moreover in the normal direction are present rotation motion due to springback;
2. the slip joint is indeed less subject to the process influence in the sliding direction, although in the normal direction are present rotation springback motions;

Parts which presents loading interference can be subjected to larger plastic deformation also at a distance from welding spots, so this condition should be avoided with a careful product and process design. It could be justified a policy to improve the dimensional quality aspects of products by favoring gap condition specifying unsymmetric tolerance on welding flanges.

Concluding, the approaches here reviewed of compliant assembly tolerance analysis cannot describe the complex behavior examined in this paper.

The calculation of the the plasticization extent is dependent on many factors, like actual part dimensions, tolerances, loading sequence, flange shape and dimensions, fixture locator position and dimension, so FE analysis are a mean suitable to deal effectively with all these variables.

To improve stack-up models for compliant assemblies, it advisable to consider:

- isotropic plastic behavior of sheet parts to be welded,
- two distinct solution models for gap and interference geometrical conditions,
- the loading sequence, contact surfaces, fixture locator position and dimensions,
- for interference condition is necessary to adopt repositioning algorithms for the parts, to correctly describe their misplacement on fixture locators,
- the welding sequence.

In real application it will also be required to adopt shell mesh elements to reduce the computation time, so it will also be necessary to transpose these results on that kind of elements.

The integration of these improvements into existing approaches like [2, 10, 13], will permit to evaluate the stiffness matrixes of each model, dependent on the deformation imposed during influence coefficient calculation to be later combined with Monte Carlo simulation so to obtain a statistical description of assemblies dimensional and geometrical quality.

References

1. Chase, Kenneth W. and Parkinson, Alan R., A survey of research in the application of tolerance analysis to the design of mechanical assemblies, Research in Engineering Design, Springer London, 1991, ISSN:0934-9839, pag. 23-37, vol. 3, issue 1, DOI:10.1007/BF01580066.
2. S.C. Liu, S.J. Hu, Variation simulation for deformable sheet metal assemblies using finite element methods, 1997, ASME Journal of Mfg. Science and Engg., v119, pp368-374.
3. S. J. Hu, Stream-of-Variation Theory for Automotive Body Assembly, Annals of the CIRP, Vol. 46/1/1997
4. S. Charles Liu, S. Jack Hu, An offset finite element model and its applications in predicting sheet metal assembly variation, International Journal of Machine Tools and Manufacture, Volume 35, Issue 11, November 1995, Pages 1545-1557, ISSN 0890-6955, DOI: 10.1016/0890-6955(94)00103-Q.
5. S. Jack Hu, Jaime Camelio, Modeling and Control of Compliant Assembly System, Annals of the CIRP, Vol. 55/1/2006
6. Jaime A. Camelio, Hyunjune Yim, Identification of dimensional variation patterns on compliant assemblies, Journal of Manufacturing Systems, Volume 25, Issue 2, 2006, Pages 65-76, ISSN 0278-6125, DOI: 10.1016/S0278-6125070006-4.
7. Minho Chang, David C Gossard, Modeling the assembly of compliant, non-ideal parts, Computer-Aided Design, Volume 29, Issue 10, October 1997, Pages 701-708, ISSN 0010-4485, DOI: 10.1016/S0010-4485(97)00017-1.
8. Min Hu, Zhongqin Lin, Xinmin Lai, Jun Ni, Simulation and analysis of assembly processes considering compliant, non-ideal parts and tooling variations, International Journal of Machine Tools and Manufacture, Volume 41, Issue 15, December 2001, Pages 2233-2243, ISSN 0890-6955, DOI: 10.1016/S0890-6955(01 00044-X.
9. Shaoyun Chen, Zhongqin Lin, Yizhu Zhang, Yoongbing Li, A parametric study of sheet metal joints for dimensional integrity, International Journal of Advanced Manufacturing Technology,

Springer London, 2006, ISSN: 0268-3768, pag. 446-452, vol. 29, issue 5, DOI: 10.1007/BF02729096

10. L. Byungwoo, M. M. Shalaby, R. J. Collins, V. Crisan, S. A. Walls, D. M. Robinson, K. Saitou, Variation Analysis of Three Dimensional non-rigid Assemblies, ISAM '07. IEEE International Symposium on Assembly and05/05 Manufacturing, 2007, pag. 13-18, ISBN: 1-4244-0563-7, DOI: 10.1109/ISAM.2007.4288442

11. R. Mantripragada, D. E. Whitney, The Datum Flow Chain: A systematic approach to assembly design and modeling, Research in Engineering Design, 1998, Springer London, volume 10, pages 150-165, ISSN:0934-9839, DOI: 10.1007/BF01607157

12. D. E. Whitney, R. Mantripragada, J. D.Adams, S. J. Rhee, Designing Assemblies, Research in Engineering Design, 1999, Springer London, volume 11, pages 229-253, ISSN:0934-9839, DOI:10.1007/s001630050017.

13. X. Fan, I. Masters, R. Roy, D. Williams, Simulation of distortion induced in assemblies by spot welding, Proceedings of the Institution of Mechanical Engineers - Part B: Journal of Engineering Manufacture, Professional Engineering Publishing, vol. 221, n. 8/2007, page 1317-1326, ISSN:0954-4054 (Print) 2041-2975 (Online), DOI: 10.1243/09544054JEM782

14. Saadat, Cretin, Sim, Najafi, Deformation analysis of large aerospace components during assembly, International Journal of Advanced Manufacturing Technology, 2009, Springer London, ISSN:0268-3768, page 145-155, vol. 41 (1), DOI:10.1007/s00170-008-1464-y.

15. Xiaoyun Liao, G. Gary Wang, Employing fractals and FEM for detailed variation analysis of non-rigid assemblies, International Journal of Machine Tools and Manufacture, Volume 45, Issues 4-5, April 2005, Pages 445-454, ISSN 0890-6955, DOI: 10.1016/j.ijmachtools.2004.09.008.

16. Xiaoyun Liao, G. Gary Wang, Wavelets-based method for variation analysis of non-rigid assemblies, International Journal of Machine Tools and Manufacture, Volume 45, Issue 14, November 2005, Pages 1551-1559, ISSN 0890-6955, DOI: 10.1016/j.ijmachtools.2005.03.001.

17. Xiaoyun Liao, G. Gary Wang, Non-linear dimensional variation analysis for sheet metal assemblies by contact modeling, Finite Elements in Analysis and Design, Volume 44, Issues 1-2, December 2007, Pages 34-44, ISSN 0168-874X, DOI: 10.1016/j.finel.2007.08.009.

18. Jaime Camelio, S. Jack Hu, Weiping Zhong, Diagnosis of multiple fixture faults in machining processes using designated component analysis, Journal of Manufacturing Systems, Volume 23, Issue 4, 2004, Pages 309-315, ISSN 0278-6125, DOI: 10.1016/S0278-6125(04)80043-8.

19. Jaime A. Camelio, S. Jack Hu, Dariusz Ceglarek, Impact of fixture design on sheet metal assembly variation, Journal of Manufacturing Systems, Volume 23, Issue 3, 2004, Pages 182-193, ISSN 0278-6125, DOI: 10.1016/S0278-6125(05 00006-3.

20. Irfan Anjum Manarvi, Neal P. Juster, Framework of an integrated tolerance synthesis model and using FE simulation as a virtual tool for tolerance allocation in assembly design, Journal of Materials Processing Technology, Volume 150, Issues 1-2, 1 July 2004, Pages 182-193, ISSN 0924-0136, DOI: 10.1016/j.jmatprotec.2004.01.036.

21. Zhijun Li, Jianpeng Yue, Michael Kokkolaras, Product Tolerance Allocation in Compliant Multistation Assembly Through Variation, ASME 2004 International Mechanical Engineering Congress and Exposition (IMECE2004), paper n. IMECE2004-60521, pp. 813-820 (8 pages), ISBN: 0-7918-4705-5, doi:10.1115/IMECE2004-60521.

22. J. A. Camelio, S. J. Hu, S. P. Marin, Compliant assembly variation analysis using component geometric covariance, Journal of Manufacturing Science and Engineering, 2004, Vol. 126, pag. 355-360, DOI: 10.1115/1.1644553

23. H. Wang, D. Ceglarek, Quality-driven Sequence Planning and Line Configuration Selection for Compliant Structure Assemblies, CIRP Annals - Manufacturing Technology, Volume 54, Issue 1, 2005, Pages 31-35, ISSN 0007-8506, DOI: 10.1016/S0007-8506(07)60043-2.

24. P.G. Maropoulos, D. Ceglarek, Design verification and validation in product lifecycle, CIRP Annals - Manufacturing Technology, Volume 59, Issue 2, 2010, Pages 740-759, ISSN 0007-8506, DOI: 10.1016/j.cirp.2010.05.005.

25. R. Soderberg, C. Wickman, L. Lindkvist, Improving decision making by simulating and visualizing geometrical variation in non-rigid assemblies, CIRP Annals - Manufacturing Technology, Volume 57, Issue 1, 2008, Pages 175-178, ISSN 0007-8506, DOI: 10.1016/j.cirp.2008.03.040.

26. H. Huh, W.J. Kang, Electrothermal analysis of electric resistance spot welding processes by a 3-D finite element method, Journal of Materials Processing Technology, Volume 63, Issues 1-3, January 1997, Pages 672-677, ISSN 0924-0136, DOI: 10.1016/S0924-0136(96)02705-7.

27. Z. Feng, S. S. Babu, M. L. Santella, B. W. Riemer, J. E. Gould, An incrementally coupled electrical-thermal-mechanical model for resistance spot welding, 5th International Conference on Trends in Welding Research, Pine Mountain, GA, 1-5 June 1998

28. J. Zhang, H. Murakawa, FEM Simulation of the Spot Welding Process (Report II). Effect of Initial Gap and Electrode-type on Nugget Formation and Expulsion, Trans JWRI (Join Weld Res Inst Osaka Univ), 1998, vol. 27, n.2, page 73-79, ISSN:0387-4508.

29. H. Eisazadeh, M. Hamedi, A. Halvaee, New parametric study of nugget size in resistance spot welding process using finite element method, Materials & Design, Volume 31, Issue 1, January 2010, Pages 149-157, ISSN 0261-3069, DOI: 10.1016/j.matdes.2009.06.042.

30. Z. Hou, I. Kim, Y. Wang, C. Li, C. Chen, Finite element analysis for the mechanical features of resistance spot welding process, Journal of Materials Processing Technology, Volume 185, Issues 1-3, ICAMT 2004 (Malaysia) & CCAMT 2004 (India) Special Issue, 30 April 2007, Pages 160-165, ISSN 0924-0136, DOI:10.1016/j.jmatprotec.2006.03.143.

31. I. Ranjbar Nodeh, S. Serajzadeh, A.H. Kokabi, Simulation of welding residual stresses in resistance spot welding, FE modeling and X-ray verification, Journal of Materials Processing Technology, Volume 205, Issues 1-3, 26 August 2008, Pages 60-69, ISSN 0924-0136, DOI: 10.1016/j.jmatprotec.2007.11.104.

32. X. Kong, Q. Yang, B. Li, G. Rothwell, R. English, X.J. Ren, Numerical study of strengths of spot-welded joints of steel, Materials & Design, Volume 29, Issue 8, 2008, Pages 1554-1561, ISSN 0261-3069, DOI: 10.1016/j.matdes.2007.12.001.

33. M. M. Rahman, R. A. Bakar, M. M. Noor, M. R. M. Rejab, M. S. M. Sani, Fatigue Life Prediction of Spot-Welded Structures: A finite element analysis approach, European Journal of Scientific Research, Vol.22 No.3 (2008), pp.444-456, EuroJournals Publishing, ISSN 1450-216X.

34. E. Feulvarch, V. Robin, J.M. Bergheau, Resistance spot welding simulation: a general finite element formulation of electrothermal contact conditions, Journal of Materials Processing Technology, Volumes 153-154, Proceedings of the International Conference in Advances in Materials and Processing Technologies, 10 November 2004, Pages 436-441, ISSN 0924-0136, DOI: 10.1016/j.jmatprotec.2004.04.096.

35. Q. Song, W. Zhang, N. Bay, An experimental study determines the electrical contact resistance in resistance welding, 2005, supplement to the Welding Journal, http://www.aws.org/wj/index.html

36. K. S. Yeung, P. H. Thornton, Transient thermal analysis of spot welding electrodes, 1999, supplement to the Welding Journal, http://www.aws.org/wj/index.html